REVISTA MATÉRIA V.30
ISSN 1517-7076 articles e20250557, 2025

Numerical study on the material removal and crack propagation mechanism of granitic rock in abrasive machining

Depeng Sun[1], Xiang Chang[1], Jinyou Kang[2]

[1]Jiangsu Vocational Institute of Architectural Technology, School of Intelligent Manufac-turing. 221116, Xuzhou, China.
[2]Ministry of Education, Key Laboratory of High-Efficiency and Clean Mechanical Manu-facture. 250061, Jinan, China.
e-mail: sun.dpeng@163.com, hichangx@163.com, jinyoukang2021@163.com

ABSTRACT

For granite materials with complex microstructure, the mechanism of subsurface crack damage and initiation and propagation in abrasive processing may not follow the classical indentation fracture mechanics theory. Consequently, research on crack initiation and propagation is centered on the microstructure of granite. The simulation model of cutting granite at grain boundary scale was established, and the mechanical response, stress field distribution, and microcrack initiation and propagation mechanism under different process parameters were studied. The results showed that the material positioned in front of the diamond grains is predominantly subjected to shear load, while the material situated below the diamond grains is primarily subjected to tensile load. Crystal boundaries have been shown to have a significant effect on crack initiation and propagation. The mechanism of crystal boundary crack systems involves dislocation accumulation at the crystal boundaries. As cutting progresses, subsurface cracks in granite undergo several processes, including dislocation excitation, dislocation movement, crystal boundary accumulation, microcrack propagation at the crystal boundaries, macro crack formation, and transgranular fracture. The number of subsurface microcracks increases with the increase in strain rate. In addition, the penetration of the intermediate crack and the internal micro-crack leads to the deviation of the intermediate crack angle.

Keywords: Abrasive machining; Cutting forces; Crystal boundary; Crack evolution.

1. INTRODUCTION

Granite is a prevalent material in the domain of building decoration and is classified as a stone variety. The limited comprehension of the processing mechanism of granite constrains the advancement of processing techniques and equipment. Granite is a paradigmatic example of a hard and brittle material. Despite the extensive research conducted on the stress field and crack evolution of fractured rock-concrete composites through numerical simulations, the majority of these studies have focused on the macroscopic scale and have primarily relied on macro mechanics for interpretation. In contrast, granite is predominantly processed through abrasive grain processing techniques, and the mechanical properties and crack evolution are predominantly explained by micromechanics. The machining mechanism of hard and brittle materials has been predominantly investigated through simulation and experimental methods [1–4]. The majority of experimental studies have utilized single diamond grains to etch the material. Subsequently, the researchers employed X-rays and SEM [5–10] to characterize the subsurface and surface of the material, respectively. Subsequent analysis was directed towards elucidating the material's removal mechanism. Nonetheless, given the prevalence of microcracks in granite, it is not feasible to analyze the subsurface through conventional inspection methods. Consequently, this study utilizes a simulation approach to investigate the material removal and crack propagation mechanism of granitic rock in abrasive machining.

The sawing of stone is defined as the removal of material achieved through the interaction of diamond grains with the material at the micrometer scale. This process differs significantly from macroscopic rock breaking. JAIME *et al*. [11] simulated the rock-cutting process using the finite element method (FEM), incorporating continuum plasticity damage mechanics and an element erosion scheme. MENEZES [12] studied the influence of friction coefficient, tool rake angle, and cutting speed on cutting forces using LS-DYNA. However, as is well known, the FEM is a continuum-based and grid-dependent simulation method, which is not ideal for modeling

Corresponding Author: Depeng Sun Received on 28/06/2025 Accepted on 12/09/2025

DOI: https://doi.org/10.1590/1517-7076-RMAT-2025-0557

heterogeneous brittle materials like rocks. Two alternative simulation methods, Smoothed Particle Hydrodynamics (SPH) and Discrete Element Method (DEM), have been shown to effectively address mesh distortion issues inherent in the FEM. In this regard, HUANG *et al*. [13] applied the DEM to analyze the crack formation and revealed the brittle-plastic transition during the rock-cutting process. AJAMZADEH *et al*. [14] investigated the effects of friction angle and accumulation coefficient on uniaxial compressive strength by the DEM. ZOU *et al*. [15] investigated the effects of cutting velocity and wedge angle on rock fragmentation using the DEM. XUE *et al*. [16] examined the influence of different joint parameters on rock fragmentation and cutting force in disc cutters through three-dimensional DEM simulations. Additionally, the SPH method, another meshless algorithm, has been used to simulate the cutting of rock materials. For example, JEONG *et al*. [17] studied the sequential cutting of rock using multiple pick cutters in the SPH framework. Despite their advantages, meshless methods such as SPH and DEM are computationally intensive due to the large number of particles involved. To address this, coupled approaches have been proposed and widely adopted. Four commonly used coupled methods include SPH-DEM [18], FEM-DEM [19], SPH-FEM [20], and SPH-DEM-FEM [21]. However, the majority of rock-cutting simulations are macro-scale focused. In stone processing, the cutting tools of diamond grains are frequently utilized, and the contact size between the tool and the workpiece generally falls within the micrometer range. Due to the variations in mechanical properties across different scales, the outcomes from macro-scale rock-cutting simulations may not be directly applicable to the diamond cutting of stone. Consequently, further refinement is imperative to establish a connection between macro-scale simulations and the micro-scale behavior observed in diamond cutting. In this regard, WANG *et al*. [19] conducted research on the abrasive machining of rock using the Finite Discrete Element Method (FDEM) to investigate the effects of cutting parameters and cutting forces.

It is a well-established fact that rocks are composed of mineral grains. However, the influence of crystal boundaries on stress field distribution and crack propagation characteristics has not yet been fully explored. The development of a theoretical model that accounts for the grain boundaries remains a significant challenge. Furthermore, experimental determination of the characteristics of crack propagation and stress field distribution is also a difficult task. To overcome these limitations, this paper investigates the material removal and crack propagation mechanism of granitic rock in abrasive machining by simulation. The novelties and contributions of the investigation can be summarized as follows:

1. The Voronoi method was utilized to establish a simulation model of diamond grain cutting granite, analyze the internal damage characteristics of abrasive cutting rock, and explore the rock cutting damage mechanism and cross-scale evolution law.
2. The dislocation stacking theory is utilized to analyze crack initiation and propagation, with a particular focus on the role of the crystal boundaries in these processes. The study elucidates the generation mechanism of transgranular cracks, providing a comprehensive understanding of the underlying mechanisms.

The remainder of this paper is organized as follows. The constitutive model and related parameters are presented in Section 2. The modeling of abrasive processing is detailed in Section 3. The results and discussion are presented in Section 4. Finally, the conclusions are presented in Section 5.

2. DETERMINATION OF THE CONSTITUTIVE MODEL AND RELATED PARAMETERS

2.1. Constitutive model

JOHNSON and HOLMQUIST [22] established the JH-2 model for ceramics. Subsequently, the model is extensively used in simulation to describe materials such as ceramics, rocks, and concrete. As shown in Figure 1(a), the strength model of the material is described. The strength of the JH-2 model is a smooth function of complete strength, fracture strength, strain rate, and damage. The strength of the normalized equivalent stress can be expressed as

$$\sigma^* = \sigma_i^* - D\,(\sigma_i^* - \sigma_f^*) \tag{1}$$

where D is the damage factor, σ_i^* and σ_f^* are the normalized intact and fractured equivalent stress, respectively.

The normalized equivalent stress of intact and completely fractured can be written as functions of the pressure and strain rate as

$$\sigma_i^* = A\,(P^* + T^*)^N\,(1 + C\ln\dot{\varepsilon}^*) \tag{2}$$

$$\sigma_f^* = B(P^*)^M (1 + C\ln\dot{\varepsilon}^*) \tag{3}$$

where A, B, C, M, and N are the rock parameters, P^* is the normalized hydrostatic pressure, $P^* = P/P_{HEL}$ T^* is the normalized maximum tensile hydrostatic pressure, $T^* = T/P_{HEL}$, P_{HEL} is the pressure at the HEL (Hugoniot elastic limit), T is the maximum tensile strength, $\dot{\varepsilon}^*$ is the normalized strain rate, $\dot{\varepsilon}^* = \dot{\varepsilon}/\dot{\varepsilon}_0$, $\dot{\varepsilon}$ is the actual strain rate of rock, $\dot{\varepsilon}_0 = 1.0\ s^{-1}$ is the reference strain rate.

As illustrated in Figure 1(b), the damage evolution of material is described. The damaged factor D is the transition of rock materials from intact to fracture strength. The expression for damage evolution can be given by

$$D = \Sigma \frac{\Delta\varepsilon^P}{\varepsilon_f^p} \tag{4}$$

$$\varepsilon_f^p = D_1 (P^* + T^*)^{D_2} \tag{5}$$

where $\Delta\varepsilon^P$ is the equivalent plastic strain within an integral cycle, ε_f^p is the equivalent plastic fracture strain of rock materials, D_1 and D_2 are the damage parameters.

As shown in Figure 1(c), the polynomial equation of state of pressure is displayed. To characterize the nonlinear deformation characteristics of rock materials under high-pressure impact, the relationship between hydrostatic pressure and volumetric strain before material damage is described using a cubic polynomial equation of state:

$$P = K_1\mu + K_2\mu^2 + K_3\mu^3 \ (\mu \geq 0) \tag{6}$$

$$P = K_1\mu \ (\mu < 0) \tag{7}$$

where K_1 is the bulk modulus, K_2 and K_3 are respectively the constants, μ is the volumetric strain, $\mu = \rho/\rho_0 - 1$, ρ and ρ_0 are respectively current and initial density, rock is subjected to tensile stress if $\mu < 0$.

Additionally, bulking occurs when rock materials fail ($D > 0$). Meanwhile, an additional pressure increment ΔP is generated by expansion energy to hydrostatic pressure.

$$P = K_1\mu + K_2\mu^2 + K_3\mu^3 + \Delta P \tag{8}$$

The pressure increment is determined from energy considerations is given by

$$\Delta P_{t+\Delta t} = -K_{1\mu+\Delta t} + \sqrt{\left(K_{1\mu_{t+\Delta t}} + \Delta P_t\right)^2 + 2\beta K_1 \Delta U} \tag{9}$$

where ΔU is the increased energy loss, β is the proportion of elastic energy loss converted to potential hydrostatic energy, $0 \leq \beta \leq 1$.

2.2. Determining the parameters of the constitutive model

Identifying the parameters of the JH-2 model is a complex process, as some constants fail to be clearly determined. The mineral content and basic parameters of brown granite are listed in our previously published paper [23].

For the JH-2 model, the *HEL* is a critical concept in the computational process. Note that the normalized parameters are derived from constants related to *HEL*, such as P_{HEL}. Consequently, the values of *HEL* should be obtained first. Generally, the mechanical response of rock materials to explosives is the measure of *HEL* [24] or a light gas gun [25]. In the field of research, *HEL* = 4.5 GPa has been a prevalent choice. Consequently, this paper has opted for *HEL* = 4.5 GPa as its standard.

Flat panel experiments can obtain the relationship between P and μ can be obtained by. The experimental data for granite was measured in literature [26–28]. The parameter K_1 can be calculated by Equation 10. After that, the fitted curve was obtained by MATLAB, as shown in Figure 2. Hence, K_2 and K_3 are obtained. Generally, the Poisson's ratio of granite is 0.29. Furthermore, the elastic modulus measured by experiments is 85 GPa. Thus, K_1, K_2, and K_3 are 67.46 GPa, 263 GPa, and −794.8 GPa, respectively.

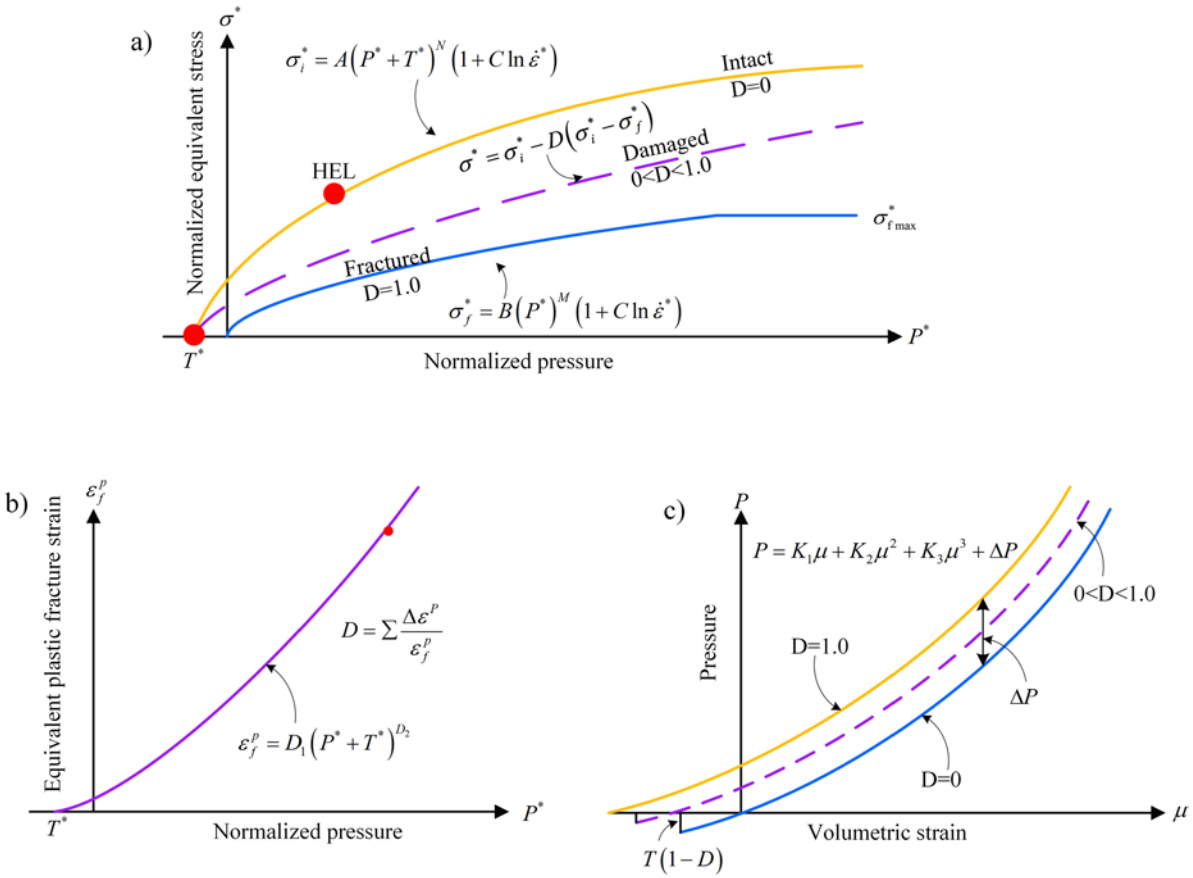

Figure 1: The JH-2 constitutive model (a) strength, (b) damage and (c) pressure.

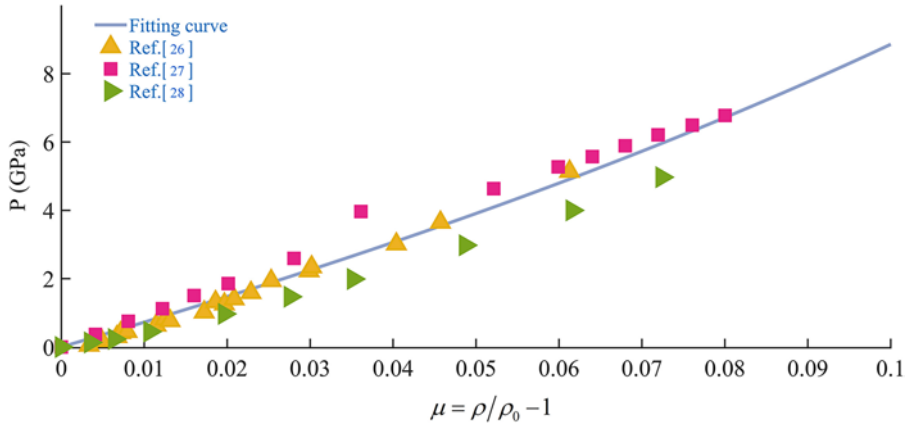

Figure 2: The relationship of P-μ for granite.

$$K_1 = \frac{E}{3(1-2\upsilon)} \tag{10}$$

where E is the elastic modulus, υ is the Poisson's ratio.

The expression of HEL can be written as

$$HEL = K_1 \mu_{HEL} + K_2 \mu^2{}_{HEL} + K_3 \mu^3{}_{HEL} + \frac{4}{3} G \frac{\mu_{HEL}}{\mu_{HEL} + 1} \tag{11}$$

Table 1: JH-2 model parameters for tan brown granite.

PROPERTIES	VALUE
Density	$\mu_0 = 2740$ kg/m^3
Modulus of elasticity	$E = 85$ GPa
Poisson's ratio	$\upsilon = 0.29$
Shear modulus	$G = 33$ GPa
HEL	$HEL = 4.5$ GPa
HEL pressure	$P_{HEL} = 2.98$ GPa
HEL volumetric strain	$\mu_{HEL} = 0.039$
Bulk modulus	$K_1 = 67.46$ GPa
Pressure coefficient	$K_2 = 263$ GPa
Pressure coefficient	$K_3 = -794.8$ GPa
Bulk factor	$\beta = 1.0$
Damage coefficient	$D_1 = 0.005$
Damage exponent	$D_2 = 0.7$
Intact strength coefficient	$A = 1.01$
Intact strength exponent	$N = 0.721$
Strain rate coefficient	$C = 0.005$
Fracture strength coefficient	$B = 0.68$
Fracture strength exponent	$M = 0.76$
Maximum fracture strength	$\sigma^* f_{max} = 0.2$ GPa
Fracture energy	$G_f = 70$ J/m^2

$$G = \frac{E}{2(1+\upsilon)} \tag{12}$$

Based on Equations 11 and 12, the value of μ_{HEL} is obtained, $\mu_{HEL} = 0.039$. Substituting μ_{HEL} into the JH-2 model calculates pressure at *HEL* of $P_{HEL} = 2.98$ GPa. Additionally, the strain rate coefficient C is assumed to be 0.005, which is the same as that of ceramics [22]. It should be pointed out that the value of the constant of C fails to significantly affect the result. Furthermore, some parameters are directly obtained from literature [29] rather than experiments. For instance, the fracture strength constants of B and M are 0.68 and 0.76, respectively, in the literature [29], and the damage parameters D_1 and D_2 were measured by JOHNSON and HOLMQUIST [22]. In summary, the relevant parameters through experiments, calculations, and references are listed in Table 1.

3. MODELLING OF ABRASIVE PROCESSING

In this study, the cutting process of granite was simulated using the Abaqus/Explicit software (Abaqus 2021). The software can handle material nonlinearities, geometric nonlinearities, and contact nonlinearities very well. A three-dimensional scratching model was developed based on a detailed analysis of the actual cutting process of granite rocks (see Figure 3), as illustrated in Figure 4. In regard to the diamond grain, the simplified model of diamond grain was designated as a rigid body, exhibiting Young's modulus of 1000 GPa, a density of 3500 kg/m^3, and a Poisson's ratio of 0.2, as documented in reference [30]. Cohesive elements were incorporated at the boundary, with a thickness of 0 μm. It is noteworthy that the unit types for the diamond grain, the cohesive elements, and the granite are C3D8R, COH3D6, and C3D4, respectively. The analysis content and process parameters (see Table 2) were defined in the analysis step. It is noteworthy that the friction coefficient between the granite and the cutting tool was found to be 0.1, as reported in the relevant literature [31].

This paper investigates the effects of process parameters on cutting forces, stress field distribution, and subsurface damage layer based on the developed model. It should be noted that the cutting angle is the counterclockwise rotation of the diamond grain (see Figure 3). The diamond grains are randomly distributed in the sawtooth or abrasive tools, and thus, three representatives of the cutting angle (see Table 2) were selected for study.

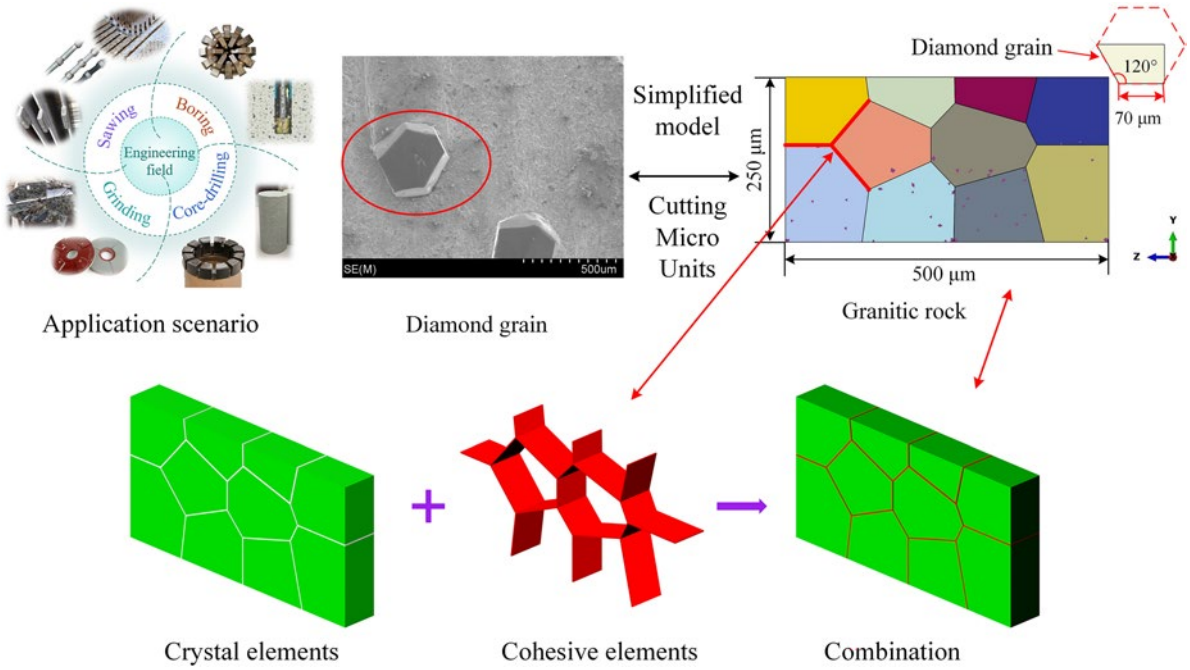

Figure 3: The ideas for simulation modeling.

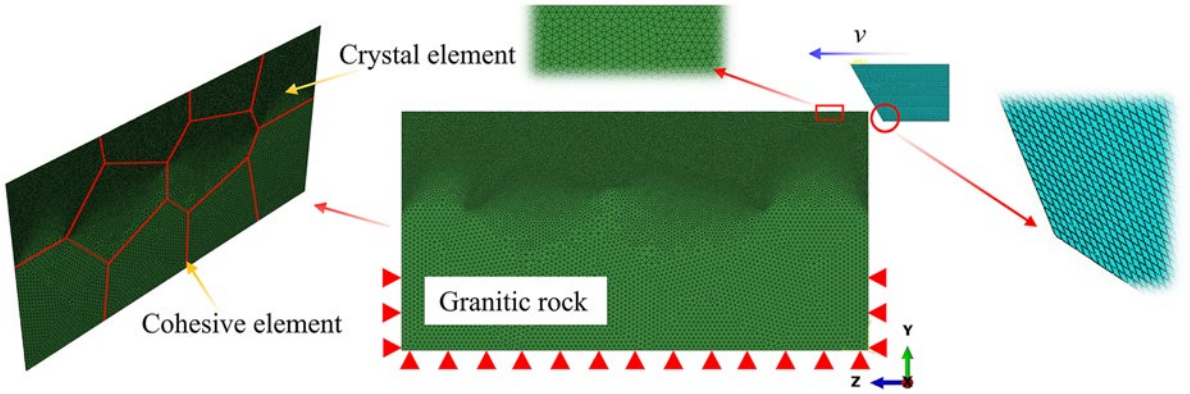

Figure 4: Pre-processing: meshing, cohesive elements, and boundary conditions.

Table 2: Process parameters in simulation.

CUTTING SPEED v	CUTTING DEPTH a_p	ANGLE θ
1 m/s	10, 20, 30 μm	0°, 15°, 30°
2 m/s	10, 20, 30 μm	0°, 15°, 30°
3 m/s	10, 20, 30 μm	0°, 15°, 30°

4. RESULTS AND DISCUSSION

4.1. Effect of cutting angle on forces and crack type

This section presents an analysis of the cutting forces under varying cutting parameters and angles. Figure 5 illustrates the cutting forces observed in the simulation for varying cutting parameters. As illustrated in the graph, there is a notable surge in cutting force as the depth of the cut rises. Similarly, a notable rise in cutting

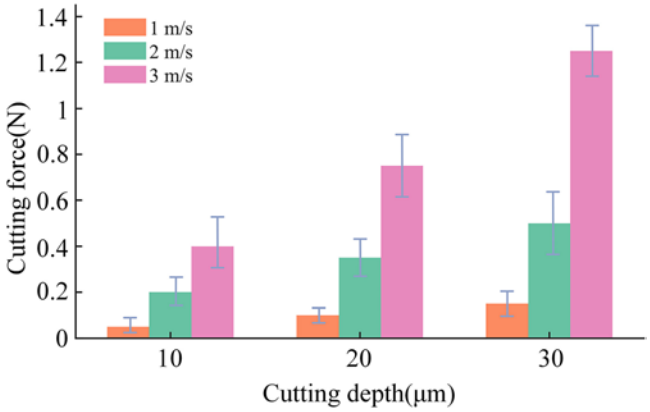

Figure 5: The cutting forces under different cutting parameters.

force is evident with an escalation in cutting speed. These results underscore the substantial impact of cutting parameters on the magnitude of cutting forces during the machining process. The material removal rate (MRR) is defined by Equation 13. As illustrated in Figure 5, the MRR can predict the general trend of cutting forces.

$$MRR = a_p \times v \times t \times b \tag{13}$$

where a_p is the cutting depth, v is the cutting speed, t is the cutting time, b is the undeformed chip width.

Previous studies have shown the importance of the random distribution of diamond grains on the surface of the grinding tool [32]. Therefore, simulations were performed to investigate the cutting forces at different cutting angles, as shown in Figure 6. Figure 6(a) shows the distribution of cutting forces and the stress field within the material for a rotation angle of the diamond grain at 0° ($\theta = 0^\circ$). Note that the waveform of the force indicates that the rock has undergone brittle fracture. The maximum principal stress is located below the front of the diamond grain and forms a semicircular ring shape. In addition, the region in front of the diamond grain, which is in contact with the rock materials, primarily experiences compressive stress, resulting in compaction of the rock material in this area. The rock material beneath the diamond grains experiences shear failure. Figure 6(b) shows the cutting forces and stress field in the material for an angle of rotation of the diamond grain of 15° ($\theta = 15^\circ$). Comparing Figure 6(a) with Figure 6(b), the tangential forces are closer to the normal forces as the angle of rotation changes. The fluctuation range of the normal forces decreases. This phenomenon may be caused by different degrees of fracture of the rock material caused by the stress fields. As shown in Figure 6(b), the maximum principal stress in front of the diamond grain forms a more obvious semicircular ring compared to Figure 6(a). In addition, the maximum shear stress decreases compared to $\theta = 0^\circ$. The rock material exhibits weakened shear deformation. As shown in Figure 6(c), when the angle of rotation is 30°, the maximum principal stress shows a more pronounced semicircular ring compared to the angle of 15°. In addition, the value of the maximum shear stress decreases, and the effective range decreases significantly. Therefore, the removal of rock material is mainly caused by type I cracks generated under tensile stress. Remarkably, Figures 6(a) and 6(b) show that the removal of rock materials is mainly caused by type I cracks generated by tensile stress and type II cracks generated by shear stress. Therefore, the orientation of the diamond grains affects the type of cracks produced during the cutting process. The rock removal process mainly involves type I cracks and composite-type cracks that occur simultaneously with type I and II cracks. This detailed analysis provides a comprehensive understanding of how changing parameters, such as rotation angle, influence the stress and crack characteristics during the rock-cutting process.

4.2. Stress field distribution characteristics

Fracture mechanics provides a fundamental mechanical tool for analyzing the removal mechanism of hard and brittle materials [33]. In order to analyze crack initiation, it is crucial to study the stress field distribution within the material. LI [34] utilised numerical methodologies to ascertain the stress field distribution beneath the indenter. In this context, the stress field was simulated during the entire scratching process, as shown in Figure 7 and Figure 8.

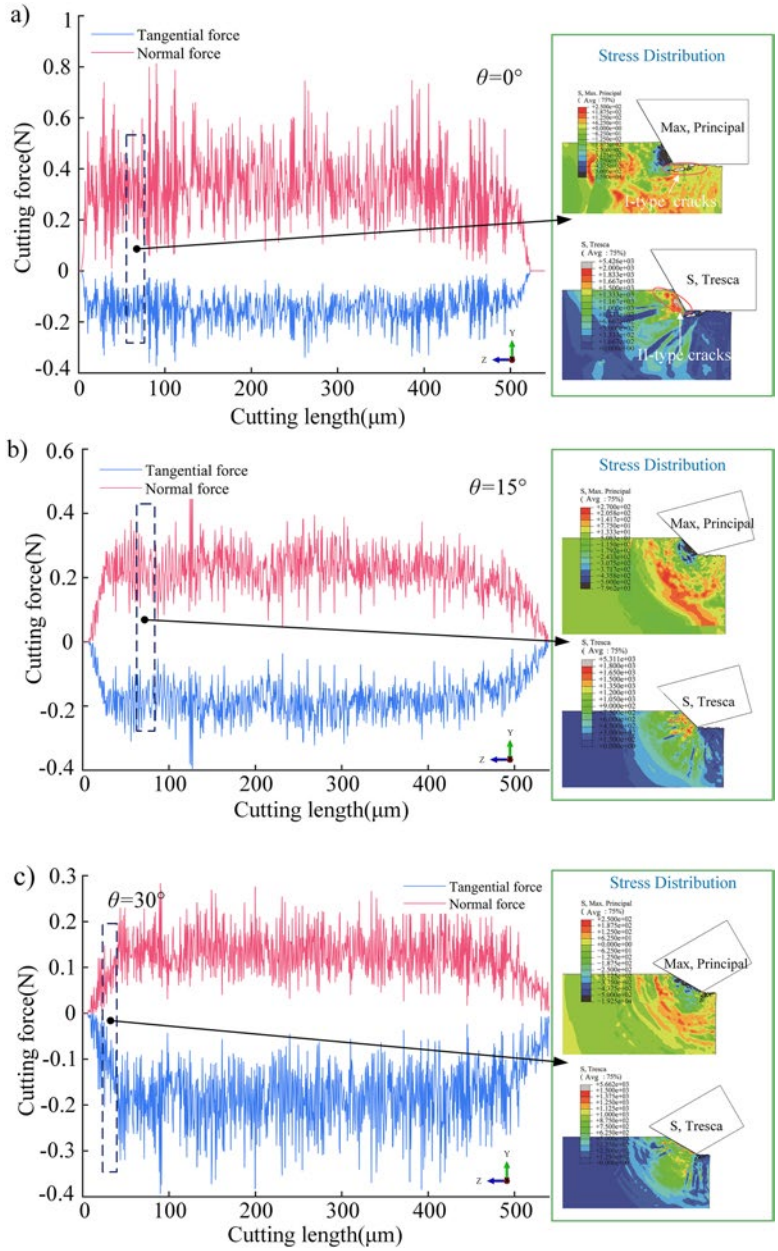

Figure 6: Cutting forces and stress distribution under different cutting angles: a_p = 20 μm, v = 2 m/s (a) θ = 0°; (b) θ = 15°; (c) θ = 30°.

Figure 7(I)–(IX) and Figure 8(I)–(IX) show the distribution of principal stress and shear stress, respectively, during the scratching process. In addition, the cutting forces are plotted together in Figure 9. Figure 7(I) shows the principal stress field as the diamond grain cuts rock materials. It is worth noting that the stress field at the crystal boundary is discontinuous, as shown in Figure 7(III). As the cutting progresses, median cracks appear on the underside of the rock material (see Figure 7(III)–(IX)). The most important result was the initial formation of median cracks on the subsurface of rock materials (see Figure 7(V)). It should be noted that the formation of median cracks occurs behind the diamond grain. That is, the expansion of the median crack is driven by residual stress. Obviously, this phenomenon is consistent with the formation mechanism of median cracks [31]. In addition, driven by residual stress, the median crack continues to propagate towards the interior of the material. (see Figure 7(V)–(IX)). As shown in Figure 7(VII)–(IX), the grain boundaries can hinder the propagation of center cracks. The principal stress occurs at the front and bottom of the diamond grain, forming a semicircular principal stress distribution area (see Figure 7). In addition, there is still a principal stress field behind the diamond grain. It seems possible that these results are due to the residual stress on the machined

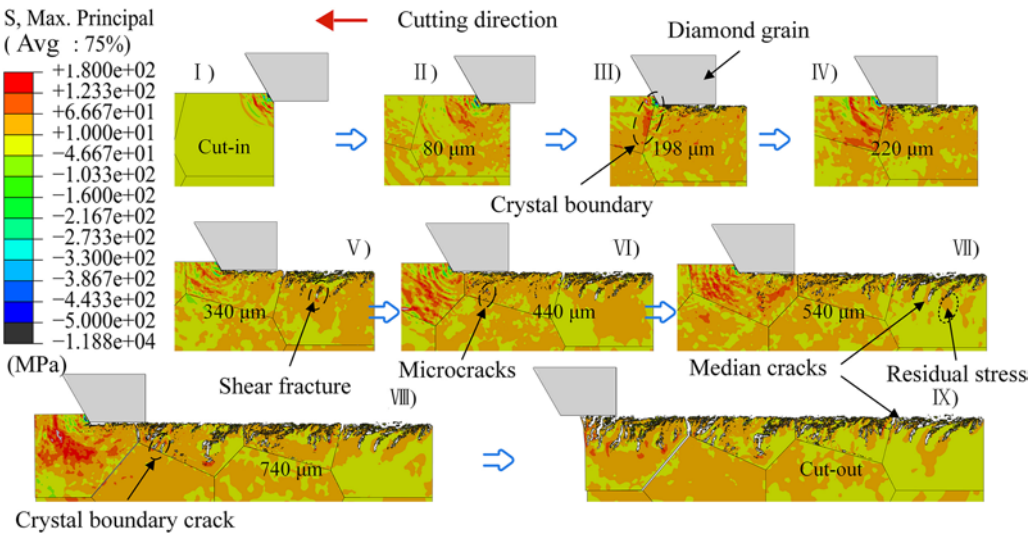

Figure 7: The principal stress distribution in dynamic cutting: a_p = 10 μm, v = 1 m/s.

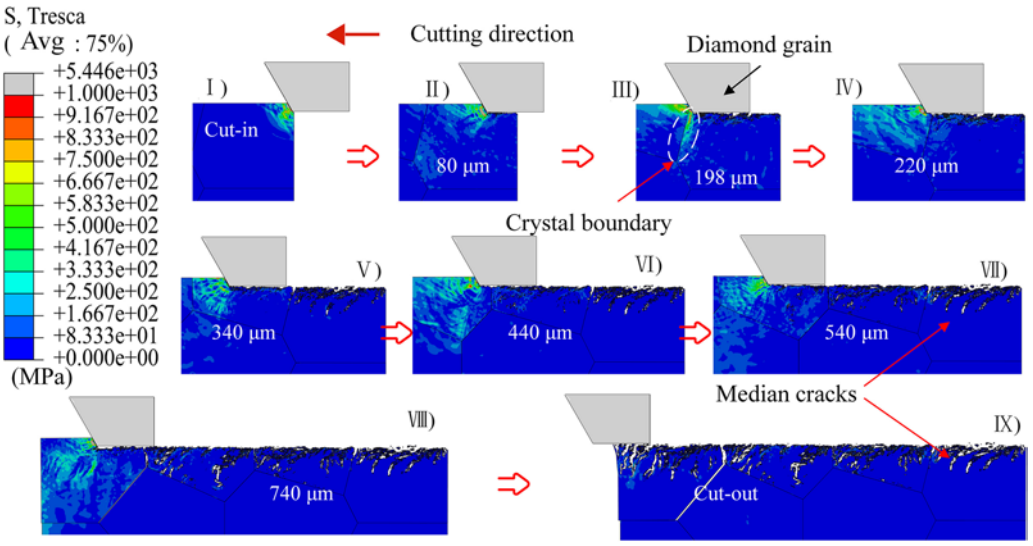

Figure 8: The shear stress distribution in dynamic cutting: a_p = 10 μm, v = 1 m/s.

surface. As shown in Figure 8(I)–(IX), shear stress occurs on the subsurface of the material in front of the diamond grit. Note that the crystal boundaries also limit the range of shear stress fields (see Figure 8(III)). As shown in Figure 7(I)–(IX), the direction of movement of the center crack and the diamond grains is at a certain angle. However, the median crack obtained from quasi-static experiments is almost perpendicular to the surface of the material, as reported in the literature [31]. However, the median cracks produced by the dynamic cutting process were deflected to a greater extent. This phenomenon underscores the importance of considering dynamic factors, such as the movement and interaction of grains during cutting processes, which may result in different crack propagation behaviors compared to static conditions. Understanding these differences is critical for accurate modeling and prediction of material removal mechanisms in dynamic cutting processes.

4.3. Subsurface damage layer

Indeed, the challenge of analyzing the correspondence between process parameters and subsurface damage layers is a common problem in materials science and engineering. Previous studies have shown that strain rate can induce material embrittlement during the loading of hard and brittle materials [9]. For example, research

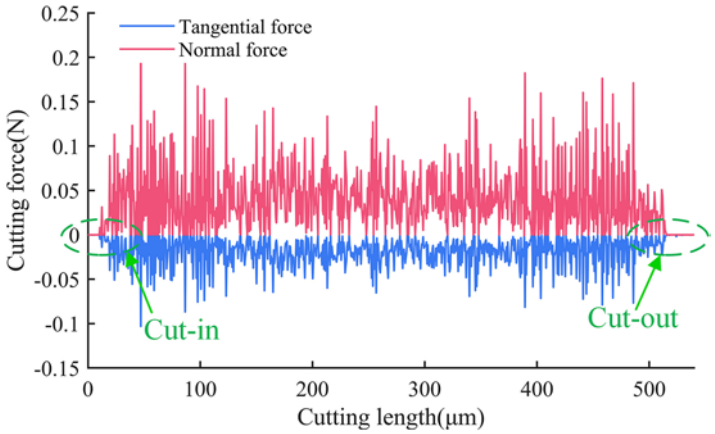

Figure 9: Cutting forces: a_p = 10 μm, v = 1 m/s.

has shown that an increase in strain rate can lead to a decrease in debris size, as documented in reference [23]. LI [35] considered strain rate analysis to investigate the lateral cracks in the material. Subsequently, a surface morphology model was established. Surface damage to the material can be observed via SEM [36]. However, the discussion of subsurface damage layers has been lacking. Therefore, to understand the subsurface damage layer, the strain rate is induced to evaluate the degree of median cracking in this paper. WANG [37] has developed a simplified formula to calculate the strain rate, which can be expressed by Equation (14). This approach offers a promising way to assess the influence of strain rate on subsurface damage and can provide valuable insight into the relationship between process parameters and material response during cutting operations. According to dislocation stacking theory, the number of microcracks in the material increases as the strain rate increases. Therefore, for the same cutting depth, the number of subsurface microcracks would also increase as the strain rate increases.

$$\dot{\varepsilon} = \frac{v}{a_p} \tag{14}$$

where v is the cutting speed, a_p is the cutting depth.

The cracks shown in Figure 10 are mainly the median cracks. According to microfracture under point indentations in brittle solids [23], the median crack is generated by the loading process of the indenter. The depth of the subsurface median crack can be calculated using Equation 15. Based on Equation 15, when the tool and material are the same, the normal force is the main factor affecting the median crack depth. Therefore, the median crack depth in Figure 10 can be explained by the normal force in Figure 5 and Equation 15 [38]. As shown in Figure 10(a)–(c), the maximum principal stress value inside the rock increases with the increase of strain rate. Therefore, the crack size at the bottom of the rock shows an increasing trend (see Figure 10(c)). As shown in Figure 10(b), (e), and (f), a cross-boundary crack has appeared inside the rock. The appearance of this phenomenon is not a through-crystal fracture but is caused by principal stresses within the crystal. The observation in Figure 10, where the angle between the median crack and the cutting direction decreases as the cutting speed increases, is interesting. In addition, the shift in the end direction of the median crack. It is important to note that this phenomenon has rarely been reported in previous literature, suggesting a new insight into the intricate relationship between cutting parameters and crack propagation behavior in hard and brittle materials.

$$C_h = C_1 \left(\frac{1}{\tan\psi} \right)^{1/3} \frac{E}{H}^{1/2} \left(F_N \right)^{1/2} \tag{15}$$

where C_h is the depth of crack, C_1 is a constant, F_N is the normal force, ψ is the half-angle of grit, E is the Elastic modulus, H is the Vickers hardness.

4.4. Mechanism of crack nucleation and propagation

The inhomogeneity of each anisotropy of the material, in conjunction with its associated content distribution, has the potential to result in inhomogeneous deformations. Consequently, in 1979, Hagan analyzed the nucleation process of the median crack based on Stroh dislocation stacking theory [39], and the dislocation stacking

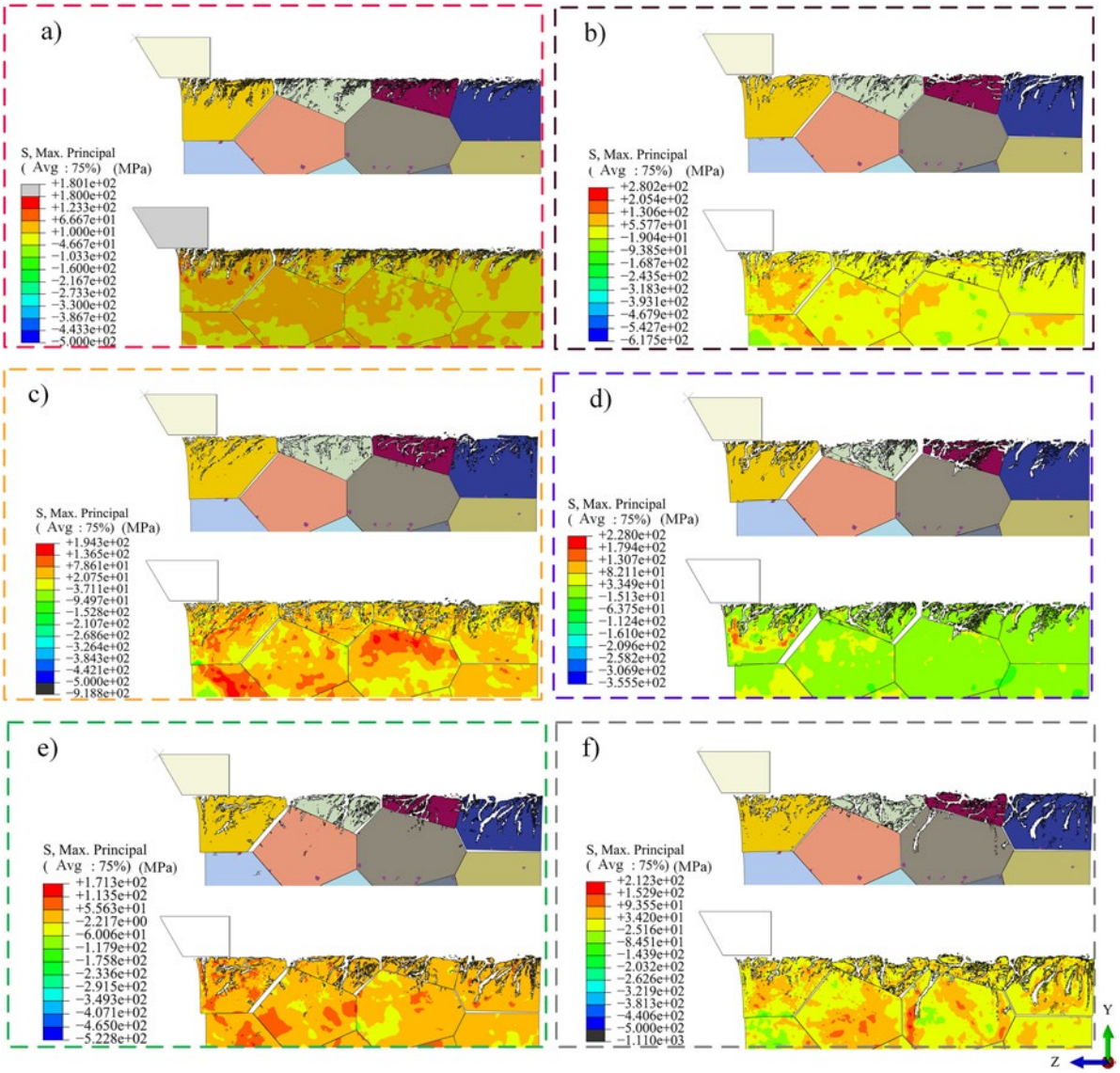

Figure 10: Stress distribution and subsurface damage layer (a) a_p = 10 μm, v = 1 m/s, $\dot{\varepsilon} = 10^5$ s^{-1}; (b) a_p = 10 μm, v = 2 m/s, $\dot{\varepsilon} = 2 \times 10^5$ s^{-1}; (c) a_p = 10 μm, v = 3 m/s, $\dot{\varepsilon} = 3 \times 10^5$ s^{-1}; (d) a_p = 20 μm, v = 1 m/s, $\dot{\varepsilon} = 5 \times 10^4$ s^{-1}; (e) a_p = 20 μm, v = 2 m/s, $\dot{\varepsilon} = 10^5$ s^{-1}; (f) a_p = 20 μm, v = 3 m/s, $\dot{\varepsilon} = 1.5 \times 10^5$ s^{-1}.

model of indentation crack was proposed. As demonstrated in Figure 11, the application of shear stress results in the displacement of dislocations from point S to point B. Prior to reaching the obstacle at point B, dislocations undergo a period of stagnation, leading to the occurrence of pinning effects. Consequently, movable dislocations within the same slip plane tend to accumulate at this point. The continuous dislocation accumulation formed a packing group, which resulted in the stress concentration at point B. The stress value exceeded the critical fracture strength threshold, thereby initiating the process of crack nucleation and subsequent expansion. As illustrated in Figures 7 and 10, the progression of internal fractures in the material during the process of diamond grain rock cutting is evident. As demonstrated in Figure 10, a substantial number of cracks are predominantly concentrated in the grains in close proximity to the processing surface and seldom extend to the subsequent layer of grains. This observation is indicative of the barrier effect of crystal boundaries on crack propagation. The movement of dislocation slip bands in the inelastic deformation zone inside the grain is often accompanied by shear fracture inside the crystal, as demonstrated in Figures 7 and 12. The generation of cracks at the grain boundary is attributable to the accumulation of dislocations at this particular location. As demonstrated in Figure 10, the crystal boundary exerts an inducing effect on the initiation of cracks. It is evident that the internal damage sustained by granite subjected to abrasive processing is predominantly characterized by two primary forms of fracture: crystal boundary cracks, which arise from dislocation accumulation at the grain boundaries, and shear fracture cracks,

which are precipitated by dislocation slip within the grains. Furthermore, as illustrated in Figures 5 and 10, it can be observed that the crack in the slip band crack system will propagate through the grain boundary to the adjacent grains under large load conditions. It is evident from Figure 10 that a proportion of the median cracks changed propagation direction during the process. This phenomenon is attributable to the continuous propagation of microcracks, which are caused by dislocation slip in the crystal and the penetration of median cracks.

At small cutting depths, the microcracks produced by shear fracture are in close proximity to the cutting layer. It has been demonstrated that an increase in both cutting depth and cutting force results in dislocations moving in close proximity to the grain boundary and accumulating there. The initiation of crack sprouting is precipitated by the stress concentration at the grain boundary, which, in turn, exceeds the material's fracture strength. This phenomenon arises as a consequence of dislocation stacking. In the presence of continuous load, microcracks are known to propagate along the crystal boundary, ultimately resulting in shear fracture. In the event of the crystal boundary cracks and microcracks extending to the machined surface, the material is subject to removal. The stress in the contact area between diamond grains and rock exceeds the strength of the rock, causing it to yield or break. In the presence of hydrostatic stress and shear stress, the occurrence of dislocation slip, twins, and stacking faults is a possibility in this area. In situations involving dynamic loading, the formation of micro-fractures within the rock matrix is a probable occurrence. The subsequent propagation of these fractures, resulting in the creation of new cracks, is a well-documented phenomenon. This process is known to induce a reduction in the hardness and strength of the rock. As demonstrated in Equation 16, there is a positive correlation between dislocation density and strain rate. Consequently, an increase in strain rate results in elevated dislocation density within the rock, leading to a rapid proliferation of microcracks and the effective absorption of impact energy. As a consequence of the expansion, evolution, and penetration of small cracks, the rock is powdered. Broken pits are evident on the machined surface and are attributed to intergranular and transgranular fractures.

Dislocation density can be expressed as [40]

$$\rho_m = \frac{\dot{\varepsilon}}{\vec{b}B_0((m_1 + n_1 \ln \dot{\varepsilon})\sigma_c)^{m^*}} \tag{16}$$

where $\vec{b}$ is the Burgers vector, $B_0 = 1/\sigma_0^{m^*}$, σ_0 is the stress with the dislocation velocity of 1 cm/s, m^* is the sensitivity index, σ_c is the critical fracture stress, m_1 and n_1 are the constant, respectively.

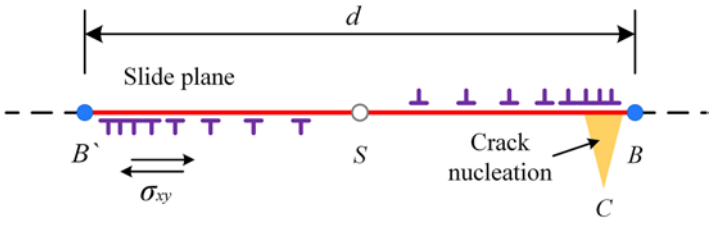

Figure 11: The nucleation of crack by dislocation pile-up.

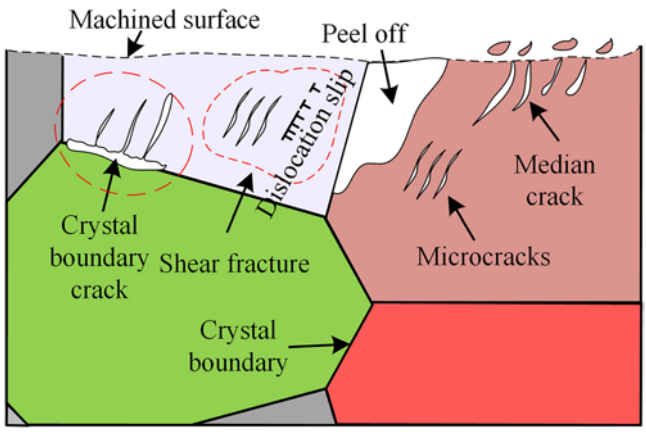

Figure 12: The schematic diagram of crack system.

5. CONCLUSIONS

In this paper, a scratching model was developed to explore the material removal and crack propagation mechanism of granitic rock in abrasive machining. Based on the model, the effects of cutting parameters, subsurface damage layer, material removal, and crack propagation mechanism were analyzed. The primary conclusions that can be drawn from this study are as follows:

(1) The material situated in front of the negative rake angle of the diamond grains is predominantly subjected to shear loading, which consequently leads to the formation of Type II cracks. Conversely, the underside of the diamond grains is primarily subject to tensile loading, resulting in the development of Type I cracks. The occurrence of Type I cracks is primarily attributed to the presence of residual stress.

(2) In the process of abrasive grit processing granite, a significant number of dislocations are known to migrate to the crystal boundary, where they accumulate, thereby initiating the formation of microcracks. These microcracks, in turn, can be induced by the crystal boundary itself. The process of crack initiation at the crystal boundary is known to be an energy-consuming phenomenon that results in the release of concentrated stress. The majority of cracks are predominantly concentrated within the grain of the cutting surface, thereby reflecting the considerable effect of grain boundaries on crack propagation.

(3) An increase in strain rate will invariably increase dislocation density. This, in turn, will lead to an increase in the number of microcracks. The interconnected nature of microcracks at crystal boundaries, microcracks generated by dislocation movement in grains, and median cracks driven by residual stress lead to the brittle removal of materials.

6. ACKNOWLEDGMENTS

This work was supported by Basic Science (Natural Science) Research Project of Higher Education Institutions in Jiangsu Province (24KJD460003).

7. BIBLIOGRAPHY

[1] WU, Y.Q., RAO, Q.J., QIN, Z.Y., *et al*., "A distinctive material removal mechanism in the diamond grinding of (0001)-oriented single crystal gallium nitride and its implications in substrate manufacturing of brittle materials", *International Journal of Machine Tools & Manufacture*, v. 203, n. 104222, pp. 104222, 2024. doi: http://doi.org/10.1016/j.ijmachtools.2024.104222.

[2] KE, J.Y., ZHANG, J.G., CHEN, X., *et al*., "Investigation on the material removal mechanism in ion implantation-assisted elliptical vibration cutting of hard and brittle material", *International Journal of Machine Tools & Manufacture*, v. 203, n. 104220, pp. 104220, 2024. doi: http://doi.org/10.1016/j.ijmachtools.2024.104220.

[3] LIU, C.H.L., KE, J.Y., YIN, T.F., *et al*., "Cutting mechanism of reaction-bonded silicon carbide in laser-assisted ultra-precision machining", *International Journal of Machine Tools & Manufacture*, v. 203, n. 104219, pp. 104219, 2024. doi: http://doi.org/10.1016/j.ijmachtools.2024.104219.

[4] YANG, X., QIU, Z.J., WANG, Y.G., "Investigation of material flow behaviour and chip formation mechanism during grinding of glass-ceramics by nanoscratch", *Ceramics International*, v. 45, n. 13, pp. 15954–15963, 2019. doi: http://doi.org/10.1016/j.ceramint.2019.05.104.

[5] YANG, X., QIU, Z.J., WANG, Y.G., "Stress interaction and crack propagation behavior of glass ceramics under multi-scratches", *Journal of Non-Crystalline Solids*, v. 523, n. 119600, pp. 119600, 2019. doi: http://doi.org/10.1016/j.jnoncrysol.2019.119600.

[6] WANG, P.Z., GE, P.Q., GE, M.R., *et al*., "Material removal mechanism and crack propagation in single scratch and double scratch tests of single-crystal silicon carbide by abrasives on wire saw", *Ceramics International*, v. 45, n. 1, pp. 384–393, 2019. doi: http://doi.org/10.1016/j.ceramint.2018.09.178.

[7] FENG, J.Y., WAN, Z.P., WANG, W., *et al*., "Scratch with double-tip tool: Crack behavior during simultaneous double scratch on BK7 glass", *Journal of the European Ceramic Society*, v. 40, n. 12, pp. 4202–4216, 2020. doi: http://doi.org/10.1016/j.jeurceramsoc.2020.04.008.

[8] LI, Z.P., ZHANG, F.H., LUO, X.C., *et al*., "Fundamental understanding of the deformation mechanism and corresponding behavior of RB-SiC ceramics subjected to nano-scratch in ambient temperature", *Applied Surface Science*, v. 469, pp. 674–683, 2019. doi: http://doi.org/10.1016/j.apsusc.2018.11.090.

[9] YANG, X.X., ZHANG, B., "Material embrittlement in high strain-rate loading", *International Journal of Extreme Manufacturing*, v. 1, n. 2, pp. 022003, 2019. doi: http://doi.org/10.1088/2631-7990/ab263f.

[10] LI, C., PIAO, Y.C., MENG, B.B., *et al*., "Phase transition and plastic deformation mechanisms induced by self-rotating grinding of GaN single crystals", *International Journal of Machine Tools & Manufacture*, v. 172, n. 103827, pp. 103827, 2022. doi: http://doi.org/10.1016/j.ijmachtools.2021.103827.

[11] JAIME, M.C., ZHOU, Y.E., LIN, J.S., *et al*., "Finite element modeling of rock cutting and its fragmentation process", *International Journal of Rock Mechanics and Mining Sciences*, v. 80, pp. 137–146, 2015. doi: http://doi.org/10.1016/j.ijrmms.2015.09.004.

[12] MENEZES, P.L., "Influence of friction and rake angle on the formation of built-up edge during the rock cutting process", *International Journal of Rock Mechanics and Mining Sciences*, v. 88, pp. 175–182, 2016. doi: http://doi.org/10.1016/j.ijrmms.2016.07.013.

[13] HUANG, H., LECAMPION, B., DETOURNAY, E., "Discrete element modeling of tool-rock interaction I: rock cutting", *International Journal for Numerical and Analytical Methods in Geomechanics*, v. 37, n. 13, pp. 1913–1929, 2013. doi: http://doi.org/10.1002/nag.2113.

[14] AJAMZADEH, M.R., SARFARAZI, V., HAERI, H., "The effect of micro parameters of PFC software on the model calibration", *Smart Structures and Systems*, v. 22, n. 6, pp. 643–662, 2018. doi: http://doi.org/10.12989/sss.2018.22.6.643.

[15] ZOU, J.Q., YANG, W.H., HAN, J.H., "Discrete Element Modeling of the Effects of Cutting Parameters and Rock Properties on Rock Fragmentation", *IEEE Access : Practical Innovations, Open Solutions*, v. 8, pp. 136393–136408, 2020. doi: http://doi.org/10.1109/ACCESS.2020.3011709.

[16] XUE, Y.D., ZHOU, J., LIU, C., *et al*., "Rock fragmentation induced by a TBM disc-cutter considering the effects of joints: A numerical simulation by DEM", *Computers and Geotechnics*, v. 136, n. 104230, pp. 104230, 2021. doi: http://doi.org/10.1016/j.compgeo.2021.104230.

[17] JEONG, H.Y., CHOI, S., LEE, S., *et al*., "Rock Cutting Simulation of Point Attack Picks Using the Smooth Particle Hydrodynamics Technique and the Cumulative Damage Model", *Applied Sciences*, v. 10, n. 15, pp. 5314, 2020. doi: http://doi.org/10.3390/app10155314.

[18] BAUMANN, A., OEZKAYA, E., SCHNABEL, D., *et al*., "Cutting-fluid flow with chip evacuation during deep-hole drilling with twist drills", *European Journal of Mechanics - B/Fluids*, v. 89, pp. 473–484, 2021. doi: http://doi.org/10.1016/j.euromechflu.2021.07.003.

[19] WANG, F.Z., LIU, S.Y., JI, K.X., "Numerical study on abrasive machining of rock using FDEM method", *Simulation Modelling Practice and Theory*, v. 104, n. 102145, pp. 102145, 2020. doi: http://doi.org/10.1016/j.simpat.2020.102145.

[20] LI, Z.T., GE, Z.L., ZHOU, Z., *et al*., "Numerical simulation and experimental verification of heterogeneous granite impacted by abrasive water jet based on SPH-FEM coupling algorithm", *Powder Technology*, v. 416, n. 118233, pp. 118233, 2023. doi: http://doi.org/10.1016/j.powtec.2023.118233.

[21] LI, B.L., WANG, C.M., LI, Y.Y., *et al*., "Dynamic Response Study of Impulsive Force of Debris Flow Evaluation and Flexible Retaining Structure Based on SPH-DEM-FEM Coupling", *Advances in Civil Engineering*, v. 2021, n. 1, pp. 9098250, 2021. doi: http://doi.org/10.1155/2021/9098250.

[22] JOHNSON, G.R., HOLMQUIST, T.J., "Response of boron carbide subjected to large strains, high strain rates, and high pressures", *Journal of Applied Physics*, v. 85, n. 12, pp. 8060–8073, 1999. doi: http://doi.org/10.1063/1.370643.

[23] SUN, D.P., ZHANG, J.S., SUN, T.Y., *et al*., "Microscale formation mechanism of surface morphology and chips features of granitic rocks considering different machining parameters", *International Journal of Advanced Manufacturing Technology*, v. 121, n. 3-4, pp. 2399–2413, 2022. doi: http://doi.org/10.1007/s00170-022-09347-1.

[24] GAUTAM, P.C., GUPTA, R., SHARMA, A.C., *et al*., "Determination of Hugoniot Elastic Limit (HEL) and Equation of State (EOS) of Ceramic Materials in the Pressure Region 20 GPa to 100 GPa", *Procedia Engineering*, v. 173, pp. 198–205, 2017. doi: http://doi.org/10.1016/j.proeng.2016.12.058.

[25] SHANG, J.L., SHEN, L.T., ZHAO, J., "Hugoniot equation of state of the Bukit Timah granite", *International Journal of Rock Mechanics and Mining Sciences*, v. 37, n. 4, pp. 705–713, 2000. doi: http://doi.org/10.1016/S1365-1609(00)00002-2.

[26] WANG, Z.J., ZHANG, D.Z., ZHANG, X.R., "Testing study on shock compression for Lantian granite", *Chinese Journal of Rock Mechanics and Engineering*, v. 22, n. 05, pp. 797–802, 2003.

[27] BRACE, W.F., RILEY, D.K., "Static uniaxial deformation of 15 rocks to 30 kb", *International Journal of Rock Mechanics and Mining Sciences & Geomechanics Abstracts*, v. 9, n. 2, pp. 271–288, 1972. doi: http://doi.org/10.1016/0148-9062(72)90028-9.

[28] SCHOCK, R.N., HEARD, H.C., STEPHENS, D.R., " Stress-strain behavior of a granodiorite and two graywackes on compression to 20 kilobars", *Journal of Geophysical Research*, v. 78, n. 26, pp. 5922–5941, 1973. doi: http://doi.org/10.1029/JB078i026p05922.

[29] AI, H.A., AHRENS, T.J., "Simulation of dynamic response of granite: A numerical approach of shock-induced damage beneath impact craters", *International Journal of Impact Engineering*, v. 33, n. 1-12, pp. 1–10, 2006. doi: http://doi.org/10.1016/j.ijimpeng.2006.09.046.

[30] LIU, S.Y., WANG, F.Z., GUO, Z.Y., *et al*., "Simulation of high-speed scratching process of marble based on finite element/discrete element coupling method", *Diamond & Abrasives Engineering*, v. 39, n. 01, pp. 95–100, 2019.

[31] WANG, W., YAO, P., WANG, J., *et al*., "Elastic stress field model and micro-crack evolution for isotropic brittle materials during single grit scratching", *Ceramics International*, v. 43, n. 14, pp. 10726–10736, 2017. doi: http://doi.org/10.1016/j.ceramint.2017.05.054.

[32] SOLTANI, H.M., TAYEBI, M., "Determination of wear parameters and mechanisms of diamond/copper tools in marble stones cutting", *International Journal of Refractory & Hard Metals*, v. 87, n. 105172, pp. 105172, 2020. doi: http://doi.org/10.1016/j.ijrmhm.2019.105172.

[33] HUANG, H., LI, X.L., MU, D., *et al*., "Science and art of ductile grinding of brittle solids", *International Journal of Machine Tools & Manufacture*, v. 161, n. 103675, pp. 103675, 2021. doi: http://doi.org/10.1016/j.ijmachtools.2020.103675.

[34] LI, C., PIAO, Y.C., ZHANG, F.H., *et al*., "Understand anisotropy dependence of damage evolution and material removal during nanoscratch of MgF2 single crystals", *International Journal of Extreme Manufacturing*, v. 5, n. 1, pp. 015101, 2023. doi: http://doi.org/10.1088/2631-7990/ac9eed.

[35] LI, C., WANG, K.C., PIAO, Y.C., *et al*., "Surface micro-morphology model involved in grinding of GaN crystals driven by strain-rate and abrasive coupling effects", *International Journal of Machine Tools & Manufacture*, v. 201, pp. 104197, 2024. doi: http://doi.org/10.1016/j.ijmachtools.2024.104197.

[36] QU, S.S., LI, L.Y., YANG, Y.Y., *et al*., "Grinding quality evaluation and removal mechanism of resin-coated SiC and 2.5D-C-SiCs surface strategies", *Tribology International*, v. 200, pp. 110181, 2024. doi: http://doi.org/10.1016/j.triboint.2024.110181.

[37] WANG, B., LIU, Z.Q., SU, G.S., *et al*., "Investigations of critical cutting speed and ductile-to-brittle transition mechanism for workpiece material in ultra-high speed machining", *International Journal of Mechanical Sciences*, v. 104, pp. 44–59, 2015. doi: http://doi.org/10.1016/j.ijmecsci.2015.10.004.

[38] LAWN, B.R., EVANS, A.G., "A model for crack initiation in elastic/plastic indentation fields", *Journal of Materials Science*, v. 12, n. 11, pp. 2195–2199, 1977. doi: http://doi.org/10.1007/BF00552240.

[39] STROH, A.N., "Dislocations and cracks in anisotropic elasticity", *Philosophical Magazine*, v. 3, n. 30, pp. 625–646, 1958. doi: http://doi.org/10.1080/14786435808565804.

[40] DAI, J.B., SU, H.H., FU, Y.C., "Effect of grinding speed on mechining damage of silicon carbide ceramics", *Jixie Gongcheng Xuebao*, v. 58, n. 21, pp. 316–330, 2022. doi: http://doi.org/10.3901/JME.2022.21.316.